Lab-scale chemical vapor deposition onto powders

Cite as: AIP Advances **12**, 075209 (2022); https://doi.org/10.1063/5.0095882
Submitted: 13 April 2022 • Accepted: 14 June 2022 • Published Online: 06 July 2022

Jun Wang and M. N. Obrovac

Lab-scale chemical vapor deposition onto powders

Cite as: AIP Advances 12, 075209 (2022); doi: 10.1063/5.0095882
Submitted: 13 April 2022 • Accepted: 14 June 2022 •
Published Online: 6 July 2022

Jun Wang[1] and M. N. Obrovac[2,3,4,a)]

AFFILIATIONS

[1] Department of Chemistry, Dalhousie University, Halifax, Nova Scotia B3H 4R2, Canada
[2] Department of Physics and Atmospheric Science, Dalhousie University, Halifax, Nova Scotia B3H 4R2, Canada
[3] Department of Process Engineering and Applied Science, Dalhousie University, Halifax, Nova Scotia B3H 4R2, Canada
[4] Clean Technologies Research Institute, Dalhousie University, Halifax, Nova Scotia B3H 4R2, Canada

[a)] Author to whom correspondence should be addressed: mnobrovac@dal.ca

ABSTRACT

In this paper, a laboratory chemical vapor deposition (CVD) reactor is described, which features an opposing screw rotating fluidized bed. The reactor efficiently concentrates powdered reactants in the reaction zone while maintaining fluidization independent of powder properties. This allows for lab-scale CVD processing of many small powder samples at high yields and without the need for re-adjustment of fluidization parameters for different samples. Alumina and graphite were carbon-coated and characterized in lithium batteries. The deposited carbon layer had a density of 1.84 g/ml and a capacity of 225 mA h/g when cycled between 7 mV and 0.9 V in lithium cells. Carbon coatings applied by this CVD reactor onto graphite particles were found to be effective at reducing surface reactions during cycling in lithium cells. We suggest that utilization of this opposing screw rotating fluidized bed reactor can effectively apply CVD coatings to small laboratory powder samples, with particular utility for Li-ion battery materials.

I. INTRODUCTION

Chemical vapor deposition (CVD) is a well-known coating technique currently in use in manufacturing and in research laboratories. There are many types of CVD methods to coat a variety of material formats. The film deposited can be in the form of metastable phases that are inaccessible by other methods; where phase formation can be carefully controlled, depending on the processing conditions.[1,2] For fine powder particle coating, efficient contact needs to be maintained between the reactive gas and the solid particles to be coated.[3] Generally, a powder CVD apparatus involves a fluidized bed in which the powder is agitated, so as to expose all powder surfaces to the reactive gas flow while maintaining the powder in the reaction zone. During processing, the reaction zone is heated (typically to temperatures above 600 °C for carbon coating), and a reactive gas flow is established (e.g., ethylene, in the case of carbon coating). Any powder that escapes the reaction zone during processing can reduce yield or, even worse, become mixed with the final product, leading to inhomogeneous coating results. Achieving an efficient fluidized bed while confining the particles to the reaction zone can be difficult to achieve, especially at the laboratory scale where samples are small (e.g., <10 g) and the reaction zone might be only a few centimeters in length.

There are two main methods of establishing a fluidized bed in a CVD reactor.[3,4] These methods are illustrated in Fig. 1. One method is by employing a rotary furnace, as shown in Fig. 1(a). This method relies on the rotation of the furnace tube to establish sample fluidization. Sample residency within the reaction zone is influenced by the rotation speed, gas flow, and by tipping the entire furnace/tube assembly. This method is particularly useful for continuous processing. When operated for batch processing small samples in the lab, the furnace angle, gas flow, and rotation speed need to be adjusted carefully to keep the particles within the reaction zone. These parameters change for different sample types and can change during CVD processing, as particle characteristics change because of thermal effects (e.g., loss of moisture at the particle surface), electrostatic charge effects, or because of changes in surface properties or aggregation due to the CVD coating. In the authors' experience, obtaining a good balance of all these parameters for a new powder sample batch is difficult, and keeping these parameters continuously

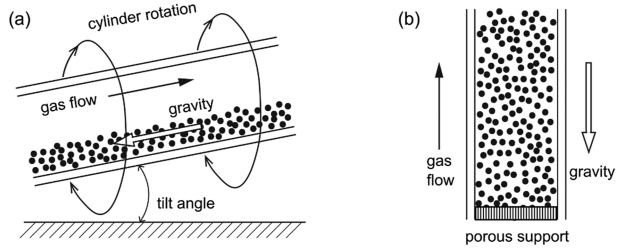

FIG. 1. Schematic diagram of (a) a rotary CVD furnace and (b) a vertical CVD furnace.

balanced during the coating process is even more challenging; often leading to low yields and inhomogeneous coating results, especially for small sample sizes.

Vertical reactors [see Fig. 1(b)] are also used for applying CVD coatings to powders, especially for small laboratory samples.[3,4] In a vertical reactor, the sample initially sits on a porous plug within the furnace tube. Reactive gas flow is adjusted to establish fluidization. In such reactors, achieving fluidization depends on the reactive gas flow, particle shape, particle density, and particle surface characteristics. Depending on the sample, fluidization may be difficult or impossible to attain or maintain, especially if the sample has a high density or has a tendency to aggregate, resulting in the gas to form channels through the powder sample, rather than uniform fluidization. As with a rotational furnace, establishing optimal parameters for new samples is challenging, as is maintaining fluidization during the CVD process. Both methods have the drawbacks of the fluidization parameters being coupled with powder properties (making it difficult to maintain fluidization as particle properties change during the CVD process) and also being coupled with the reactive gas flow (limiting CVD reaction conditions based on reactive gas flows necessary to maintain fluidization). For the above reasons, CVD processing using conventional horizontal rotational reactors or vertical reactors is highly challenging at the laboratory scale, where typically many small batches of materials, each often having different properties, need to be processed.

One application of CVD powder processing is the carbon coating of graphite powders for use as active negative electrode materials in Li-ion batteries. Both artificial and natural graphites are utilized. Despite its lower cycle life, natural graphite is utilized extensively as the negative electrode in Li-ion batteries because of its low cost. However, due to its relatively active edge structure, natural graphite can easily react with electrolyte during Li-ion battery operation. This can cause electrolyte decomposition reaction products to accumulate on the graphite surface, forming a solid electrolyte interphase (SEI). Continual growth of the SEI during cell operation can lead to increased battery internal resistance and lithium consumption. Both of these effects can, in turn, result in capacity loss. Coating both artificial and natural graphites with carbon can reduce surface reactivity, resulting in reduced SEI growth and increased cycle life.[5]

This article describes a CVD reactor for laboratory use that utilizes a unique rotating reaction tube that can achieve fluidization of small particle batches, regardless of the powder properties, while efficiently confining the sample to a small reaction zone. To test and apply this lab-made apparatus, an aluminum oxide sample and a graphite sample were carbon-coated successfully by using ethylene gas as a carbon source. From these samples, the density and the electrochemical properties in lithium cells of the coated carbon layer were determined. It was found that this reactor system can be used for CVD coating small batches of different powders without the need for any optimization of the fluidized bed, making it ideal for laboratory use.

II. EXPERIMENTAL

A. The CVD reactor

The CVD reactor utilized in this study was designed to confine small amounts of fluidized powder to the reaction zone of a furnace, irrespective of the powder properties. This was accomplished with a rotating reactor tube having internal fins in an opposing screw configuration. The CVD reactor is shown schematically in Fig. 2(a). It consists of the following:

1. A rotating quartz tube with inner opposing screws ~120 cm in length with an inner diameter of 25 mm. During tube rotation, the opposing screws efficiently fluidize the sample powder while simultaneously concentrating the powder in the reaction zone in the middle of the tube.
2. A laboratory tube furnace with a ~25 cm heating zone.
3. An electric motor with a speed controller to drive the tube.
4. Rotation joints with gas feed throughs.
5. Mineral oil bubblers to provide gas seals and keep a constant pressure in the reaction tube.
6. Ar gas source.
7. Ethylene gas source.
8. A gas flow meter.

B. CVD procedure

5 ml (3 ml based on true density) of Al_2O_3 powder (600 mesh Aluminum Oxide Grit from Kramer Industries Inc.) or graphite powder (MesoCarbon MicroBeads, from China Steel Chemical Co., particle size ~26 μm) was carefully placed at the center of the CVD furnace tube. Glass filter paper was packed into the furnace tube outlet to stop tar from accumulating in the exhaust gas lines. The loaded tube was assembled into the CVD setup, according to Fig. 2(a) and was purged with Ar gas (60 ml/min.) for 1 h. While still under Ar gas flow, tube rotation was started at ~100 rpm and the temperature was increased to 800 °C in 30 min. The Ar gas flow was then stopped, and a flow of ethylene gas was established through the tube at 80 ml/min for the desired CVD processing time (e.g., 5 h), while the tube was under constant rotation and heated at 800 °C. The flow of ethylene gas was then stopped, Ar was reintroduced in the tube at 60 ml/min, and the furnace was allowed to cool. Rotation was stopped only after the sample reached room temperature. Samples were carefully collected from the furnace tube without contamination from accumulated downstream tar.

C. Material characterization

X-ray diffraction (XRD) patterns were measured using a Rigaku Ultima IV powder diffractometer X-ray system equipped with a Cu

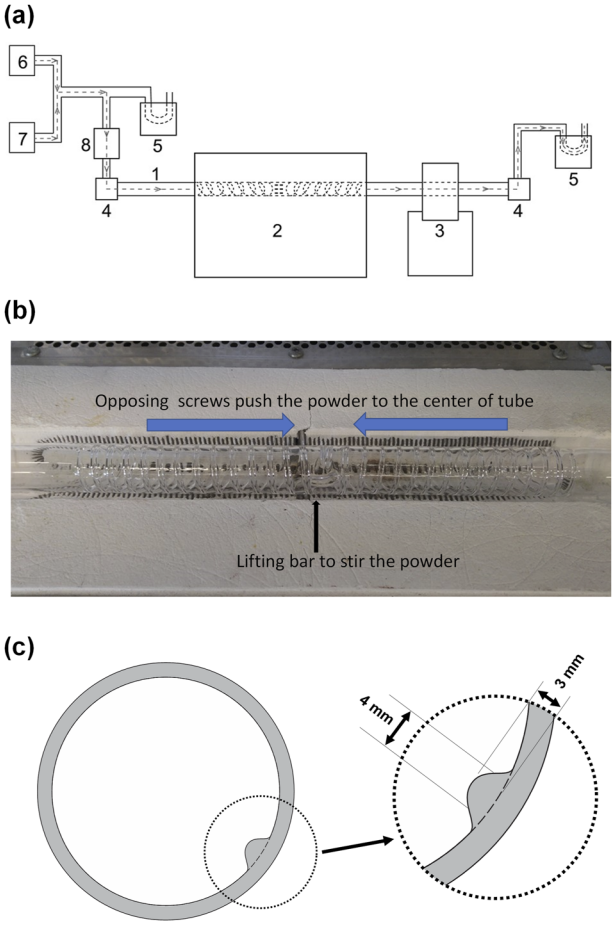

FIG. 2. (a) A schematic diagram of the opposing screw rotating fluidized bed CVD setup. The opposing screw reactor tube is shown in detail with arrows indicating the direction of powder flow toward the center of the tube (where lifter bars are located) during tube rotation. (b) A photograph of the opposing screw reactor tube centered in the heated zone of a furnace. (c) Cross section of opposing screw reactor tube with an inset showing the profile of a screw fin in detail.

Kα X-ray source, a diffracted beam monochromator, and a scintillation detector. Each XRD pattern was collected from 10° to 80° 2-theta in 0.05° increments for 3 s per step. Laser Raman spectroscopic measurements were performed in the 1200–1700 cm^{-1} region with a laser radiation wavelength of 532 nm and a power of 15 mW using a HORIBA T64000 Raman spectrophotometer. Sample powder cross sections were prepared with a JEOL Cross-Polisher (JEOL Ltd., Tokyo, Japan) and sample powder morphologies were studied with a TESCAN MIRA 3 LMU variable pressure Schottky field emission scanning electron microscope (SEM) at 5.0 and 20.0 kV. The sample densities were measured with dry helium gas using a Micromeritics AccuPyc II 1340 gas pycnometer. Thermal gravimetric analysis (TGA) was conducted using a NETZSCH TG 209F3 thermogravimetric analyzer with compressed air as purge gas (flow rate: 20 ml/min), in a heating range from 20 to 800 °C with 10 °C/min heating rate. A summary of the coated carbon content, true density, and Brunauer–Emmett–Teller (BET) surface area of the samples prepared in this study is provided in Table I.

TABLE I. Coated carbon content, true density, and BET surface area of the samples prepared in this study.

Sample	Coated carbon content (wt. %)	True density (g/cm^3)	Surface area (m^2/g)
Al_2O_3	0%	3.98	0.39
C–Al_2O_3(5 h)	13%	3.46	0.50
Graphite	0%	2.18	0.29
C-Gr(1 h)	10%	2.14	0.20
C-Gr(2 h)	19%	2.10	0.19

D. Electrochemical characterization

C–Al_2O_3(5 h) electrode slurries were prepared from C–Al_2O_3(5 h), carbon black (Super C65, Imerys Graphite and Carbon), and lithium polyacrylate (LiPAA) [from a 10 wt. % LiPAA aqueous solution, made by neutralizing a polyacrylic acid solution (Sigma–Aldrich, the average molecular weight of 250 000 g mol^{-1}, 35 wt. % in water) with LiOH·H_2O (Sigma–Aldrich, 98%)] in a volumetric ratio of 70/5/25 (corresponding to an 83/4/13 weight ratio) with a few drops of wetting agent (isopropanol, Sigma–Aldrich, 99.5%) in distilled water. C-Gr electrode slurries were prepared from C-Gr, carbon black, and polyvinylidene fluoride binder (PVDF, Kynar HSV 900) in a mass ratio of 96/2/2 with an appropriate amount of *N*-methyl-2-pyrrolidone (NMP, Sigma–Aldrich, anhydrous 99.5%) to establish a good slurry viscosity. Slurries were mixed using a high-shear mixer equipped with a Cowles blade at 5000 rpm for 10 min and then spread onto the electrolytic copper foil (Furukawa Electric, Japan) with a 0.1 mm gap coating bar. The coatings were dried in air at 120 °C for 40 min, punched into 1.3 cm (in diameter) disks, and then heated under vacuum for a few hours at 120 °C with no further air exposure before cell assembly.

Electrodes were assembled into 2325-type coin cells with a lithium foil (Aldrich, 99.9%) counter/reference electrode separated by two layers of separators (Celgard 2300) in an Argon filled glove box. 168 μl of electrolyte was used in each half cell. The electrolyte consisted of 1M $LiPF_6$ (BASF) in a solution of ethylene carbonate (EC), diethyl carbonate (DEC), and mono-fluoroethylene carbonate (FEC) (volume ratio 3:6:1, all from BASF). Cells were cycled at 30 °C between 7 mV and 0.9 V using a Neware battery testing system at a C/10 rate for the first cycle and a C/5 rate for the following cycles. Cells were held at 7 mV after discharge (lithiation) until a rate decreased to C/20 for the first cycle or C/10 for subsequent cycles, to simulate constant current-constant voltage (CCCV) charging in a full cell. Electrochemical impedance spectra (EIS) were measured using a Bio-Logic VMP3 potentiostat/EIS spectrometer. EIS measurements were performed at 20 °C with a 10 mV amplitude excitation and a frequency range from 100 kHz to 10 mHz.

III. RESULTS AND DISCUSSION

The opposing screw reactor tube is shown in detail in Fig. 2(b). It consists of a quartz tube to which inner fins (also quartz) have been

fused to form opposing screws. A cross section of the tube showing the profile of a screw fin and its approximate dimensions is shown in Fig. 2(c).

When rotated during operation, the screws confine the sample powder to the center of the tube while fluidizing the powder mixture. An additional quartz lifter bar at the center of the tube enhances fluidization further. This CVD reactor design provides an effective fluidized bed, while simultaneously confining even very small sample amounts within the reaction zone (a video of a fluidized powder sample confined in our rotating opposing screw reactor tube is provided as supplementary material). This is a significant improvement over traditional CVD methods, especially for small sample sizes. Moreover, unlike traditional horizontal rotating tube or vertical tube fluidized beds, no adjustment was needed between particle samples with different morphologies, compositions, and densities. This enables rapid CVD processing of many different small samples, which is typically needed for materials development.

Carbon-coated samples utilizing the CVD reactor are denoted here using the following notation "C–Al_2O_3(5 h)" for carbon-coated Al_2O_3 and "C-Gr(2 h)" for carbon-coated graphite, where the quantity in brackets is the CVD processing time. Al_2O_3 particles were carbon-coated to characterize the nature of the carbon deposited by the reactor. Figure 3(a) shows an SEM image of uncoated Al_2O_3. The Al_2O_3 particles are about 9 (D10)–20 (D90) μm in size, with a median (D50) size of 14 μm. The particles are irregularly shaped, with smooth sides and sharp edges. The BET surface area of these particles was measured to be 0.39 m^2/g. Using the measured density of these particles of 3.98 g/ml, this corresponds to a volumetric surface area of 1.55 m^2/ml. After 5 h carbon coating [Fig. 3(b)], the resulting C–Al_2O_3(5 h) particles are uniformly covered with a thick carbon layer, excepting a few areas in which the coating has flaked off. We have noted that carbon coatings can flake off smooth substrates, especially when they become thick (>0.1 μm). Figure 3(c) shows an SEM image of cross-sectioned C–Al_2O_3(5 h) particles. Except where flaking has occurred, the particle surfaces are completely coated with a dense carbon layer that is about 0.2–0.7 μm in thickness. EDS maps of C, Al, and O [Figs. 3(d)–3(f), respectively] more clearly show the encapsulation of the Al_2O_3 particles within a pure carbon layer that has little oxygen content.

XRD patterns of the Al_2O_3 and C–Al_2O_3(5 h) samples are shown in Fig. 4. Carbon coating has resulted in the appearance of a broad XRD peak near 24°, characteristic of a disordered carbon.[6] A Raman spectrum of the C–Al_2O_3(5 h) sample is shown in Fig. S1. The most prominent feature of the spectrum being a sharp peak at about 1590 cm^{-1}. This peak corresponds most closely with the G band of single walled carbon nanotubes (SWCNT), which are commonly made by CVD processing.[7] Another sharp peak near 1480 cm^{-1} is close to the most prominent peak in the Raman spectrum of C_{60}.[8] The most prominent broad features near 1340 and 1580 cm^{-1} correspond to the D and G bands of graphite.[9] The large D band compared to the G band indicating a highly disordered carbon.[10] Smaller broad features in the Raman spectrum could not be identified. These features and features similar to those of SWCNT, C_{60}, and disordered carbon suggest the deposited carbon is a complex mixture of metastable and disordered phases.

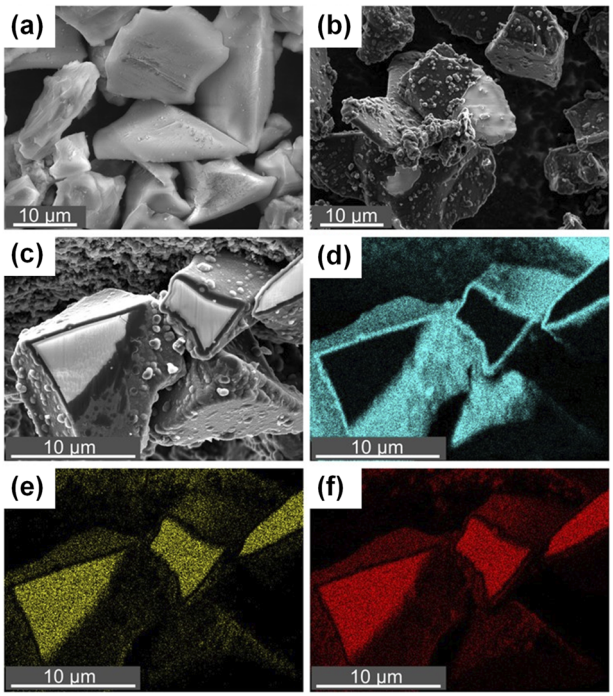

FIG. 3. SEM images of (a) uncoated Al_2O_3 powder and (b) C–Al_2O_3(5 h). (c)–(f) SEM images of cross-sectioned C–Al_2O_3(5 h) particles and corresponding EDS mappings of C, Al, and O elements, respectively.

The C–Al_2O_3(5 h) sample was used to determine the density, porosity, and electrochemical properties of the coated carbon. The amount of coating present on the C–Al_2O_3(5 h) particles was determined to be 13 wt. % by thermogravimetric analysis (Fig. 5). Helium pycnometry determined the C–Al_2O_3(5 h) sample density to be

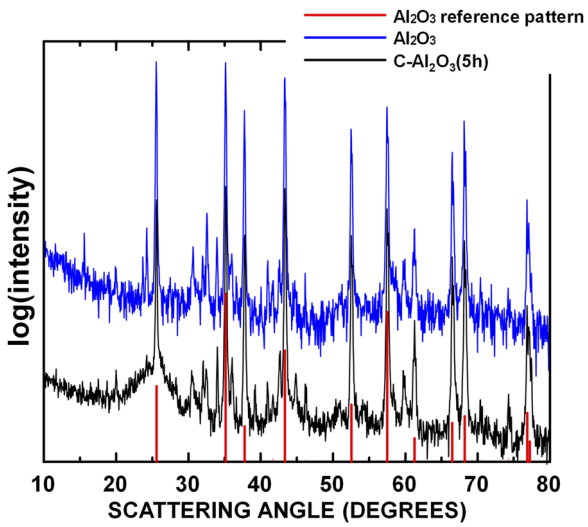

FIG. 4. XRD patterns of Al_2O_3 and C–Al_2O_3(5 h).

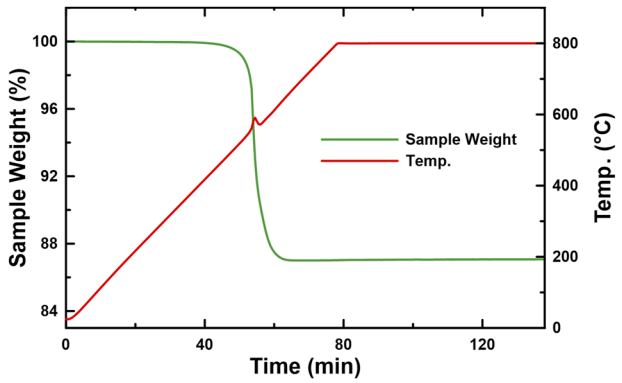

FIG. 5. The weight loss of C–Al_2O_3(5 h) during heating in air at a constant heating rate.

3.46 g/ml. From the TGA and pycnometry results, the density of coated carbon was calculated to be 1.84 g/ml. Assuming a uniform coating on the 0.39 m^2/g Al_2O_3 particles, a 13 wt. % 1.84 g/ml carbon coating corresponds to an average coating thickness of 0.2 μm, which is consistent with SEM observations. The BET surface area of C–Al_2O_3(5 h) was measured to be 0.50 m^2/g or 1.73 m^2/ml. This represents an 11% increase in volumetric surface area compared to the Al_2O_3 precursor particles. This higher value is likely due to the carbon coating that delaminated from the sample in some areas, as mentioned above, resulting in the formation of thin carbon flakes. Such thin flakes will have a high surface area, and therefore, their presence would cause an increase in overall surface area.

Since Al_2O_3 is electrochemically inactive in Li-cells, the C–Al_2O_3(5 h) sample was used to evaluate the electrochemical properties of the carbon coating. Figure 6(a) shows the potential profile of C–Al_2O_3(5 h). The profile is typical of a disordered carbon (i.e., either a hard carbon or partially pyrolyzed soft carbon, see, for example, Ref. 11). The cycling performance is shown in Fig. 6(b). The carbon coating has a specific capacity of around 225 mA h/g, with no detectible loss of capacity and a high CE of 99.95% after 100 cycles.

Figure 7(a) shows an SEM image of uncoated graphite powder. The graphite particles are roughly spherical and are about 19 (D10)–39 (D90) μm in size, with a median (D50) size of 27 μm. The true density of the graphite powder was measured to be 2.18 g/ml. This low value compared to the crystallographic density of graphite (2.26 g/ml) is indicative of internal porosity that is inaccessible to the helium gas used in the density measurement. The BET surface area of the graphite was measured to be 0.29 m^2/g or 0.63 m^2/ml. The graphite particle surfaces are mostly smooth on the scale of the image shown in Fig. 7(a); however, ridges and pits on the surface are clearly visible. Figure 7(b) shows an SEM image of C-Gr(1 h). The surface morphology has changed to nodular, with none of the features of the underlying graphite surface visible. Figure 7(c) shows an SEM image of C-Gr(2 h). With extended carbon coating time, the nodules have elongated into spikes. In addition, the particles have begun to aggregate (Fig. S2). Figure 7(d) shows an SEM image of a cross section of a C-Gr(2 h) particle. The particles are completely coated with carbon, having an average coating thickness is about 1 μm.

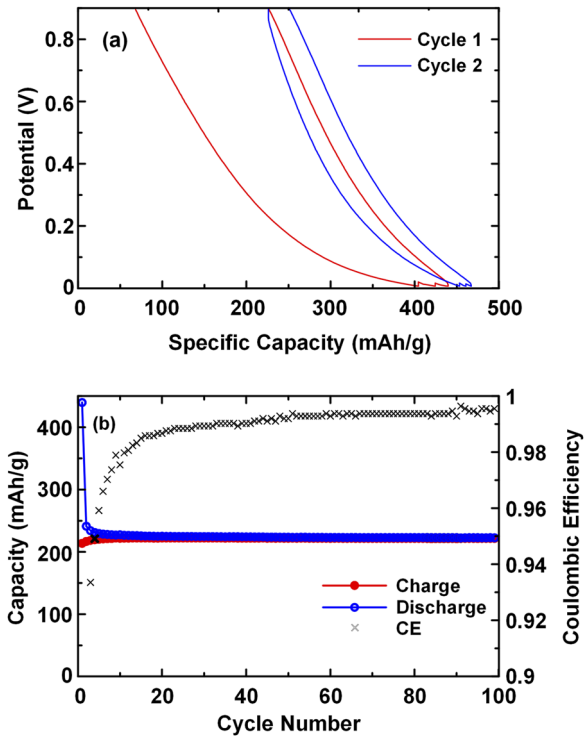

FIG. 6. (a) Potential profile and (b) cycling performance of C–Al_2O_3(5 h). Here, the capacity is plotted in units of mA h per gram of carbon.

The BET surface area of the C-Gr(1 h) particles was measured to be 0.2 m^2/g. This represents the lower limit of detection of the BET instrument; therefore, the actual sample surface area may be even lower. Even so, this represents a considerable reduction (31%) compared to the surface area of the original graphite particles. We

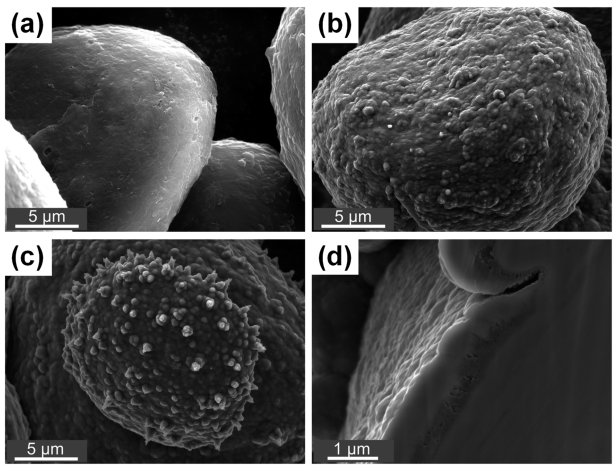

FIG. 7. SEM images of (a) graphite, (b) C-Gr(1 h), (c) C-Gr(2 h), and (d) cross-sectioned C-Gr(2 h).

believe that this large reduction in surface area is due to a combination of the low surface area of the coated carbon plus the effect of pore closure. This can be seen in Fig. S3, where internal porosity in the graphite has been closed off by the carbon coating. The density of the C-Gr(1 h) particles was 2.14 g/ml. If the carbon coating has the same 1.84 g/ml density as determined from the C–Al_2O_3(5 h) sample, this density reduction of the C-Gr(1 h) compared to uncoated graphite corresponds to a 10% by weight carbon coating. After 2 h of CVD processing, the density reduces further to 2.10 g/ml, corresponding to a 19% by weight carbon coating. Despite the formation of spiky nodules, the C-Gr(2 h) sample's surface area remains near the lower detection limit of the BET instrument (0.19 m^2/g or 0.40 m^2/ml).

To evaluate the effectiveness of the carbon coating in improving the cycling characteristics of graphite in Li cells, graphite electrodes were made uncalendared and with low carbon black and binder content. Such coatings have poor electrical conductivity, resulting in exacerbated impedance growth. Figure 8 shows the potential profiles and differential capacity curves of the 1st, 50th, and 100th cycle of graphite, C-Gr(1 h), and C-Gr(2 h) electrodes. Initially, all potential profiles are similar, and the differential capacity curves show distinct staging peaks. By cycle 50, there is a capacity loss for the uncoated graphite and C-Gr(1 h) with an increase in cell polarization, indicative of impedance growth, while the potential profile of C-Gr(2 h) remains almost unchanged. By cycle 100, the polarization of the uncoated graphite electrode has become extremely severe, and distinct staging plateaus are no longer visible, while the CVD coated electrodes have much less polarization and still show distinct staging plateaus. These changes are evident in the capacity vs cycle life of these electrodes, as shown in Fig. 9. All electrodes have a similar initial capacity of about 350 mA h/g. During cycling, the uncoated graphite electrode suffers continual fade with ~35% loss in capacity after 100 cycles. As shown in Fig. 8, this loss of capacity is due to increased polarization. The cycling of the C-Gr(1 h) cell is only

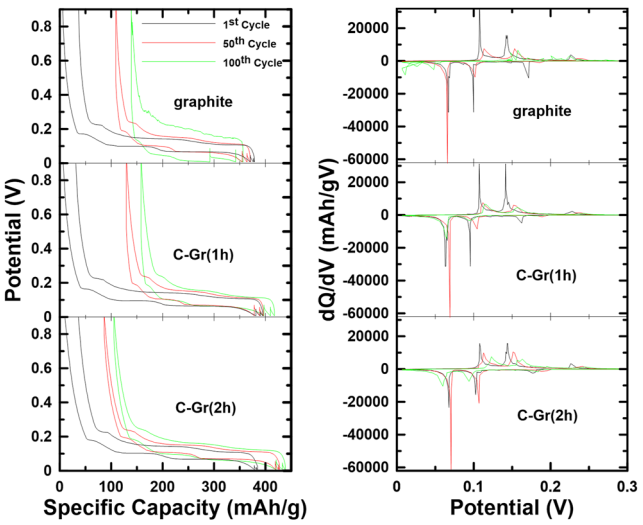

FIG. 8. Potential profiles and differential capacity curves of graphite and C-Gr samples.

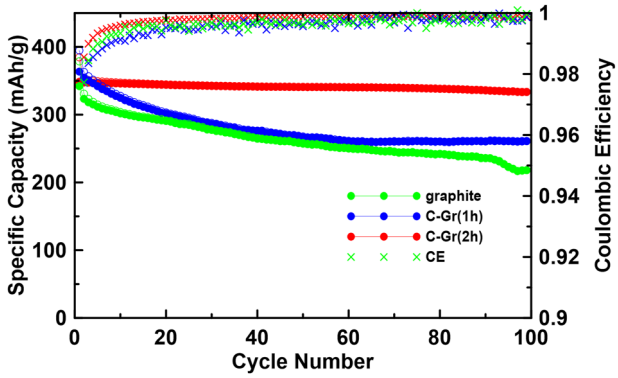

FIG. 9. Cycling performance of graphite and C-Gr samples.

slightly improved. Both the graphite and C-Gr(1 h) have similar Coulombic efficiencies (CE, also shown in Fig. 9), which increase during cycling, presumably improving as the SEI layer thickens. Evidently, the 1 h CVD coating was not sufficient to significantly impact SEI growth. In contrast, the C-Gr(2 h) electrode shows almost no fade, little polarization growth, and a higher CE throughout cycling.

Despite the large differences in cell polarization observed during cycling, EIS spectra of the graphite, C-Gr(1 h), and C-Gr(2 h) samples (Fig. S4) show relatively small differences in cell impedance. These spectra are typical of graphite electrodes, consisting of two semicircles, the first in the high frequency region being ascribed to lithium-ion diffusion through the SEI layer and the semicircle in the medium-to-low frequency being ascribed to the transfer resistance. The total real impedance of the C-Gr(2 h) sample is slightly smaller than the C-Gr(1 h) and graphite samples, but this is not significant enough to account for the large differences in polarization and fade observed in Figs. 8 and 9. This indicates that the primary mechanism for failure in the graphite and C-Gr(1 h) cells may be due to graphite exfoliation from solvent co-intercalation. This is known to increase cell polarization, but can simultaneously cause the graphite surface area to increase, resulting in little change or even a decrease in charge transfer resistance.[12] It is well known that carbon coating can effectively inhibit solvent co-intercalation into graphite,[13] which is likely the primary mechanism by which polarization is reduced and cycling is improved in the C-Gr(2 h) sample.

IV. CONCLUSIONS

A lab-scale CVD apparatus has been developed with a fluidized bed that can efficiently contain small amounts (~3 ml, based on true density) of powdered samples in a furnace reaction zone. Furthermore, samples with different densities, particle shapes, and particle sizes are contained in the reaction zone without any adjustment of the fluidized bed. The reactor was used to carbon coat a small (5 ml) sample of graphite particles, resulting in a uniform carbon coating that was shown to effectively inhibit electrolyte reactivity when the coated graphite was utilized as a negative electrode in Li cells. The ability to efficiently deposit continuous and even coatings onto small particle samples shown here presents a significant improvement over other CVD methods, which have difficulty processing small samples

and in which the fluidized bed must be readjusted and optimized depending on powder properties. We believe that this presents an enormously useful tool for exploratory research in fields such as battery materials, where many small powder samples of active electrode materials must be synthesized for the investigation of trends in materials properties and for rapid materials optimization. In addition, we have observed that this fluidized bed design can be used to synthesize unique composite materials, which we will report in later publications.

SUPPLEMENTARY MATERIAL

See the supplementary material for figures showing a Raman spectrum of the C–Al_2O_3(5 h) sample; SEM images of C-Gr(2 h) showing particle aggregation; an SEM image of a cross-sectioned C-Gr(2 h) particle, showing pore closure due to the carbon-coated layer; and EIS spectra of graphite, C-Gr(1 h), and C-Gr(2 h) samples after 50 cycles and measured at 0.9 V.

ACKNOWLEDGMENTS

The authors acknowledge financial support from NSERC and NOVONIX Battery Technology Solutions Inc. under the auspices of the NSERC Alliance Grants program (Grant No. AG ALLRP 558364-20). A Jobin Yvon T64000 Raman spectrometer located in the lab of Dr. K. C. Hewitt, Dalhousie University, Department of Physics and Atmospheric Science (e-mail: Kevin.Hewitt@Dal.ca, phone: 902-494-2315) was used to obtain some of the results presented in this paper. The instrument is funded by the Canada Foundation for Innovation and the Natural Sciences and Engineering Research Council of Canada and is part of a user facility available to industrial or academic researchers.

AUTHOR DECLARATIONS

Conflict of Interest

The authors have no conflicts to disclose.

Author Contributions

Jun Wang: Data curation (equal); Formal analysis (equal); Investigation (equal); Methodology (equal); Validation (equal); Writing – original draft (equal); Writing – review & editing (equal). **M. N. Obrovac:** Conceptualization (equal); Data curation (equal); Project administration (equal); Supervision (equal); Validation (equal); Writing – review & editing (equal).

DATA AVAILABILITY

The data that support the findings of this study are available from the corresponding author upon reasonable request.

REFERENCES

[1]F. Li, R. Tao, B. Cao, L. Yang, and Z. Wang, Adv. Funct. Mater. **31**, 2104367 (2021).
[2]X. Luo, Z. Peng, Z. Wang, and M. Dong, ACS Appl. Mater. Interfaces **13**, 59154 (2021).
[3]C. Vahlas, B. Caussat, P. Serp, and G. Angelopoulos, Mater. Sci. Eng., R **53**(1), 1 (2006).
[4]G. Takashi and K. Hirokazu, in *Handbook of Solid State Chemistry*, 1st ed., edited by R. Dronskowski, S. Kikkawa, and A. Stein (Wiley-VCH, Verlag, 2017), Vol. 2, pp. 399–428.
[5]H. Li and H. Zhou, Chem. Commun. **48**, 1201 (2012).
[6]Y.-S. Ding, W.-N. Li, S. Iaconetti, X.-F. Shen, J. DiCarlo, F. S. Galasso, and S. L. Suib, Surf. Coat. Technol. **200**, 3041 (2006).
[7]S. Suzuki and H. Hibino, Carbon **49**, 2264 (2011).
[8]A. Talyzin and U. Jansson, Thin Solid Films **350**, 113 (1999).
[9]A. Cuesta, P. Dhamelincourt, J. Laureyns, A. Martínez-Alonso, and J. M. D. Tascón, Carbon **32**, 1523 (1994).
[10]S. Reich and C. Thomsen, Philos. Trans. R. Soc., A **362**, 2271 (2004).
[11]J. R. Dahn, A. K. Sleigh, H. Shi, J. N. Reimers, Q. Zhong, and B. M. Way, Electrochim. Acta **38**(9), 1179 (1993).
[12]C. Wang, A. J. Appleby, and F. E. Little, Electrochim. Acta **46**, 1793 (2001).
[13]H. Wang and M. Yoshio, J. Power Sources **93**, 123 (2001).